



This is a peer-reviewed, post-print (final draft post-refereeing) version of the following published document:

Li, Pengzhi ORCID logoORCID: <https://orcid.org/0000-0001-8883-1885>, Wang, Xiao-Dong, Zhao, Lei, Zhang, De-Fu and Guo, Kang (2019) Dynamic linear modeling, identification and precise control of a walking piezo-actuated stage. Mechanical Systems and Signal Processing, 128. pp. 141-152. doi:10.1016/j.ymssp.2019.03.037

Official URL: <https://doi.org/10.1016/j.ymssp.2019.03.037>

DOI: <http://dx.doi.org/10.1016/j.ymssp.2019.03.037>

EPrint URI: <https://eprints.glos.ac.uk/id/eprint/9068>

Disclaimer

The University of Gloucestershire has obtained warranties from all depositors as to their title in the material deposited and as to their right to deposit such material.

The University of Gloucestershire makes no representation or warranties of commercial utility, title, or fitness for a particular purpose or any other warranty, express or implied in respect of any material deposited.

The University of Gloucestershire makes no representation that the use of the materials will not infringe any patent, copyright, trademark or other property or proprietary rights.

The University of Gloucestershire accepts no liability for any infringement of intellectual property rights in any material deposited but will remove such material from public view pending investigation in the event of an allegation of any such infringement.

PLEASE SCROLL DOWN FOR TEXT.



UNIVERSITY OF
GLOUCESTERSHIRE

This is a peer-reviewed, post-print (final draft post-refereeing) version of the following published document:

Li, Pengzhi ORCID: 0000-0001-8883-1885, Wang, Xiao-Dong, Zhao, Lei, Zhang, De-Fu and Guo, Kang (2019) Dynamic linear modeling, identification and precise control of a walking piezo-actuated stage. Mechanical Systems and Signal Processing, 128. pp. 141-152. doi:10.1016/j.ymssp.2019.03.037

Official URL: <https://doi.org/10.1016/j.ymssp.2019.03.037>

DOI: <http://dx.doi.org/10.1016/j.ymssp.2019.03.037>

EPrint URI: <http://eprints.glos.ac.uk/id/eprint/9068>

Disclaimer

The University of Gloucestershire has obtained warranties from all depositors as to their title in the material deposited and as to their right to deposit such material.

The University of Gloucestershire makes no representation or warranties of commercial utility, title, or fitness for a particular purpose or any other warranty, express or implied in respect of any material deposited.

The University of Gloucestershire makes no representation that the use of the materials will not infringe any patent, copyright, trademark or other property or proprietary rights.

The University of Gloucestershire accepts no liability for any infringement of intellectual property rights in any material deposited but will remove such material from public view pending investigation in the event of an allegation of any such infringement.

PLEASE SCROLL DOWN FOR TEXT.

Dynamic linear modeling, identification and precise control of a walking piezo-actuated stage

Peng-Zhi Li^{a,b,*}, Xiao-Dong Wang^{a,*}, Lei Zhao^{a,b}, De-Fu Zhang^a, Kang Guo^a

^a*Changchun Institute of Optics, Fine Mechanics and Physics, Chinese Academy of Sciences, Changchun 130033, China*

^b*University of Chinese Academy of Sciences, Beijing 100049, China*

Abstract

In this paper, a dynamic model is firstly investigated for a flexible mechanical stage driven by a walking piezoelectric actuator (WPA). The developed model takes into account the WPA, the mechanical stage and moreover the connection part between them as an overall piezo-actuated stage. The model of the WPA is derived mainly from the electrical, piezoelectric and mechanical sides. Besides, the WPA and mechanical stage are treated as elements with lumped mass. Then the proposed model is identified based on the open-loop frequency response data. Finally, hybrid closed-loop controllers are designed for point-to-point (PTP) positioning and sinusoidal trajectory tracking control of the overall piezo-actuated stage. The hybrid control strategy includes displacement error feedback and velocity feed-forward control algorithms. Furthermore, the transient profile and tracking differentiator is proposed for quick settling of PTP positioning control, and the discrete-time repetitive controller (RC) is adopted to enhance the tracking precision for the periodic sinusoidal trajectory. Experimental results show that for the 300 μm PTP positioning the settling time is 0.12 s to keep the steady error within 25 nm, and for the sinusoidal trajectory of 50 μm amplitude the maximum tracking error is 1.99%. These results clearly demonstrate the high precision performance of the developed hybrid controllers for the walking piezo-actuated stage.

Keywords: walking piezoelectric actuator, frequency response, hybrid

*Corresponding authors. Tel.: +86 431 8670 8156/8199; Fax: +86 431 8670 8158.

Email addresses: lipengzhi@ciomp.ac.cn (Peng-Zhi Li), wangxd@ciomp.ac.cn (Xiao-Dong Wang)

1. Introduction

The piezoelectric actuator (also referred as PZT) is mainly composed of the lead-zirconate-titanate piezoelectric ceramics. Generally, the stacked piezoelectric actuator will change about 0.1% of their static length when an electric field is applied due to the inverse piezoelectric effect. Because the piezoelectric actuator can move linearly with the nano-meter displacement resolution, it is widely used in micro-/nano-positioning [1, 2, 3, 4, 5, 6] and optics [7, 8, 9, 10]. However, the stacked piezoelectric actuator often has the travel stroke limitation of about one hundred microns.

Hence, the walking piezoelectric actuator (WPA) shows its advantage of a few millimetres travel stroke while still maintaining the nano-meter displacement resolution. It moves like the inchworm creature by alternate movement of two or more pairs of piezoelectric legs. The walking principle of the investigated WPA is of the non-resonant type, which assures very good control of the motion over the whole travel range. Refs. [11], [12] and [13] proposed some static and dynamic models for the WPA, but with few attention to the model of the overall piezo-actuated stage. Regarding the control issues, Ref. [12] adopted the gain scheduling feedback in combination with feed-forward control to improve the performance of the WPA driven stage. Ref. [13] presented a virtual time control method based on the coordinate transformation. Ref. [14] proposed a delay-varying repetitive control scheme and applied it to a nano-motion stage driven by the WPA. In Ref. [15], an explicit force controller has been developed based on a statistically linear system model for the compensated WPA. The proposed controllers are mainly designed for step or jogging movement of the WPA or the WPA driven stage.

This paper develops a dynamic model taking into account the WPA, the mechanical stage and moreover the connection part between them as an overall piezo-actuated stage. And hybrid closed-loop controllers are designed for point-to-point (PTP) positioning and sinusoidal trajectory tracking control of the overall WPA driven stage. Furthermore, the transient profile and tracking differentiator is proposed for quick settling of PTP positioning control, and the discrete-time repetitive controller (RC) [4, 14, 16, 17] is adopted for precise periodic sinusoidal trajectory tracking control. For now, there are seldom public literatures reporting the experimental results of sinusoidal trajectory tracking control for the overall WPA driven stage.

The organization of this paper is as follows. Section 1 gives a brief introduction. In Section 2, we propose the dynamic model for the overall stage driven by the WPA. Section 3 shows the experimental setup. Section 4 is presented with the model identification. Section 5 includes the controller design and experimental results. In Section 6, a summary of the paper is given.

2. Modeling

2.1. Introduction of the WPA

As shown in Fig. 1, the movement of the WPA is introduced by its rod and virtually generated by its 2 pairs of legs [18]. The WPA is mainly composed of a rod, 2 or more pairs of piezoelectric legs and the corresponding leg tips. The piezoelectric legs can elongate or bend when excited by external voltages. A pair of piezoelectric legs is usually comprised of 2 piezoelectric legs, i.e. P_{1A} and P_{1B} form the first pair of legs, and P_{2A} and P_{2B} compose the second pair of legs. A piezoelectric leg is comprised of 2 piezoelectric multilayer-stacked actuators. The WPA moves step by step described as follows:

- First, all 4 piezoelectric legs are electrically excited and elongate in contact with the rod in Fig. 1a.
- Second, the first pair of legs (P_{1A} and P_{1B}) maintains contact with the rod and moves right. The second pair of legs (P_{2A} and P_{2B}) retracts and their tips bend left in Fig. 1b.
- Third, P_{2A} and P_{2B} in turn elongate and come into contact with the rod. Their tips move right. Meanwhile, P_{1A} and P_{1B} retracts and their tips bend left in Fig. 1c.
- Last, P_{2A} and P_{2B} move right. P_{1A} and P_{1B} begins to elongate and move up towards the rod in Fig. 1d.

Different electrical voltage waveforms will affect the step length and moving motion behaviour of the WPA. The adopted waveform for smooth stepping motion is shown in Fig. 2. Generally, one piezoelectric leg is electrically excited by two channels of voltages with the same profile but different phases, which makes the piezoelectric leg move like the bimorph cantilever. Besides, the same pair of legs is electrically excited by the same voltages. That is to

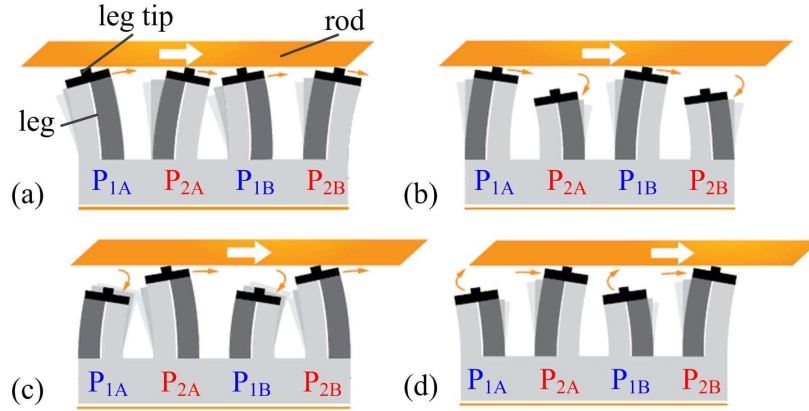


Figure 1: The working principle of the WPA.

say, the piezoelectric leg P_{1A} is electrically excited by V_1 and V_2 , and P_{1B} of the same first pair is also electrically excited by V_1 and V_2 . Similarly, P_{2A} and P_{2B} are identically electrically excited by V_3 and V_4 . The frequency of the voltage waveform corresponds to the moving velocity of the WPA.

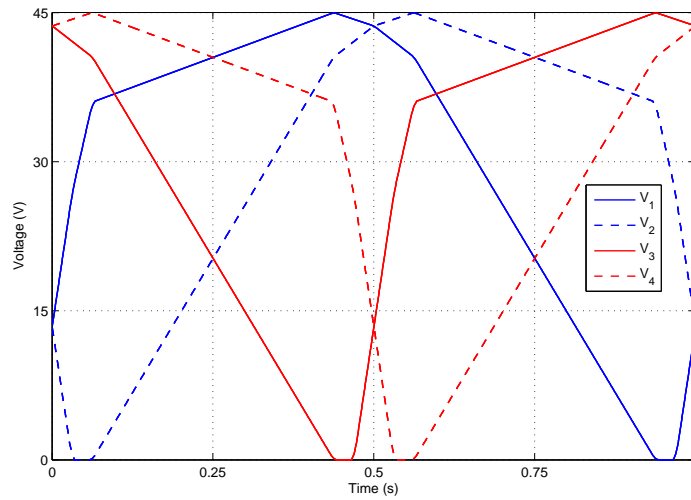


Figure 2: The voltage waveform for electrically exciting the WPA.

2.2. Dynamic linear model of the overall piezo-actuated stage

The schematic representation of the dynamic linear model of the overall piezo-actuated stage is shown in Fig. 3. The presented model consists of 3 parts: WPA, connection and mechanical stage. The model of the WPA is derived mainly from the electrical, piezoelectric and mechanical sides. Besides, the WPA and mechanical stage are treated as elements with lumped mass. It should be also noted that for the sake of simplicity, the hysteresis effect and the converted back electromagnetic field from the mechanical side are not included in the model of the WPA.

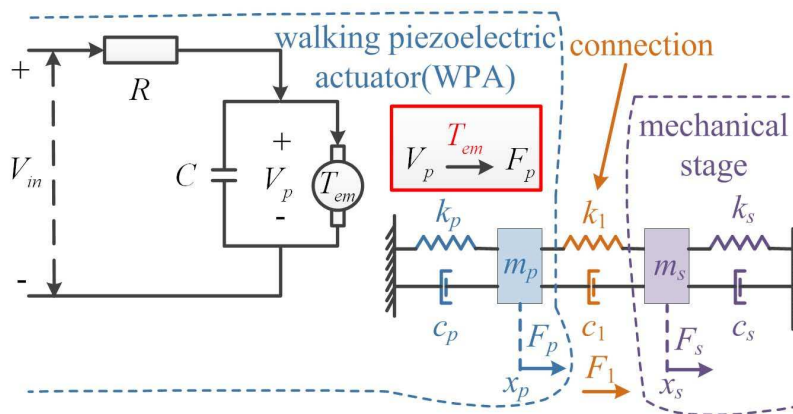


Figure 3: The schematic representation of the dynamic linear model of the overall piezo-actuated stage.

The model of the WPA can be approximately described as follows:

$$V_{in} = V_p + RC\dot{V}_p \quad (1)$$

$$V_p T_{em} = F_p \quad (2)$$

$$F_p - F_1 = m_p \ddot{x}_p + c_p \dot{x}_p + k_p x_p \quad (3)$$

where V_{in} and V_p are the total exerted and piezoelectric transformed voltages, R is the equivalent electrical resistance mainly from the power source and the power amplifier, C is the equivalent capacitance of the WPA in the x_p direction, T_{em} is the electromechanical transformation ratio due to the piezoelectric effect, F_p is the internal force transformed from the electrical side because of the piezoelectric effect, F_1 is the external force applied to the WPA from the connection part, x_p is the displacement of the moving

rod of the WPA, m_p , c_p and k_p are the equivalent lumped mass, damping coefficient and stiffness of the WPA in the x_p direction from the mechanical domain respectively.

The lumped mass-spring-damper model of the connection part and mechanical stage can be represented in the following equations:

$$F_1 = c_1 (\dot{x}_p - \dot{x}_s) + k_1 (x_p - x_s) \quad (4)$$

$$F_1 + F_s = m_s \ddot{x}_s + c_s \dot{x}_s + k_s x_s \quad (5)$$

where c_1 and k_1 are the equivalent damping coefficient and stiffness of the connection part, m_s , c_s and k_s are the equivalent lumped mass, damping coefficient and stiffness of the mechanical stage in the x_s direction same as x_p direction respectively, and F_s is the external force applied to the mechanical stage.

The transfer function from V_{in} to F_p can be obtained by taking Laplace transformations of Eq. (1) and Eq. (2) in the following equation

$$\frac{F_p(s)}{V_{in}(s)} = \frac{T_{em}}{1 + RCs} \quad (6)$$

where s is the Laplace variable.

In the same way, substituting the Laplace transformations of Eq. (3) and Eq. (4) into that of Eq. (5) with $F_s = 0$ yields the transfer function from F_p to x_s

$$\frac{x_s(s)}{F_p(s)} = \frac{c_1 s + k_1}{(m_p s^2 + c_p s + k_p) (m_s s^2 + (c_1 + c_s) s + k_1 + k_s) + (m_s s^2 + c_s s + k_s) (c_1 s + k_1)} \quad (7)$$

At last, substituting Eq. (6) into Eq. (7) gives the transfer function from V_{in} to x_s as

$$\frac{x_s(s)}{V_{in}(s)} = \frac{T_{em}}{1 + RCs} \cdot \frac{c_1 s + k_1}{(m_p s^2 + c_p s + k_p) (m_s s^2 + (c_1 + c_s) s + k_1 + k_s) + (m_s s^2 + c_s s + k_s) (c_1 s + k_1)} \quad (8)$$

In the practical implement of the overall piezo-actuated stage, the input voltage u_{in} to the power amplifier is interpreted as the frequency of the exciting voltage waveform, thus corresponding to the moving velocity of the stage. As a result, an integral element with a gain k_u is added, and the final transfer function of the overall piezo-actuated stage from the input voltage u_{in} to the displacement x_s of the stage becomes

$$\frac{x_s(s)}{u_{in}(s)} = \frac{k_u}{s} \cdot \frac{T_{em}}{1 + RCs} \cdot \frac{c_1s + k_1}{(m_p s^2 + c_p s + k_p)(m_s s^2 + (c_1 + c_s)s + k_1 + k_s) + (m_s s^2 + c_s s + k_s)(c_1 s + k_1)} \quad (9)$$

Hence, the order of the proposed dynamic linear model for the walking piezo-actuated stage is 6 and will be used for the identification in the next Section. For the sake of simplicity and linear modelling, non-linear characteristics of the overall stage such as hysteresis and friction are not considered for now. It is worth pointing out different values of k_1 and c_1 of the connection part will affect the dynamic characteristic of the overall stage. Suppose $s_{1,2p}$ and $s_{1,2s}$ are the roots of the polynomials $m_p s^2 + c_p s + k_p$ and $m_s s^2 + c_s s + k_s$ respectively, then they will not be the poles of the transfer function in Eq. (9). That is to say, the sole first-order natural frequencies of the WPA and mechanical stage will not be the ones of the overall stage.

3. Experimental platform configuration

As shown in Fig. 4, a flexure-hinge based mechanical stage driven by the WPA is built as the experimental platform. The mechanical stage of 1 degree of freedom has a nominal displacement of 0-500 μm , which can be measured by the capacitive sensor. Customized from PiezoMotor Uppsala AB in Sweden, the WPA is electrically excited by the power amplifier (MC-90) with 4 channels of output voltages. The displacement value of the capacitive sensor (CSH05-CAm1,4) is electronically processed by the signal conditioner (capaNCDT 6500) with a pre-amplifier (CPM6011). The sensor and its signal conditioner are supplied by Micro-Epsilon Company in Germany. Provided by A&D Company in Japan, the real-time platform (AD5436A) is used for high-speed measurement and rapid control prototyping. It contains CPU board with real-time operating system, 16 bits A/D and 16 bits D/A converter boards. The terminals are used for connecting the WPA and sensor

signal conditioner with the real-time platform. The piezo-actuated stage with the capacitive sensor is fixed on a vibration isolation mounting. The laboratory is under precise environmental control with its ambient temperature kept at 22 ± 0.2 degree Celsius.

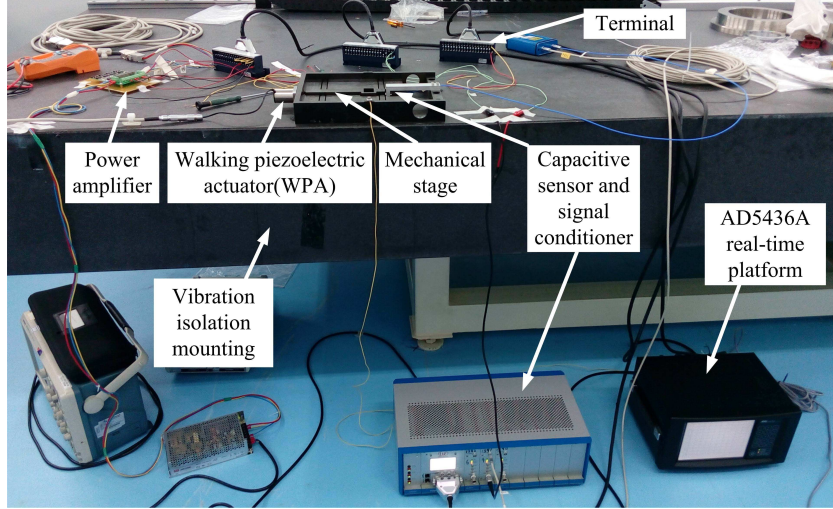


Figure 4: Experimental platform with the mechanical stage, the power amplifier, the WPA, the capacitive sensor and the real-time platform.

4. Identification

Not only the model of the WPA but also that of the mechanical stage and the connection part have great influences on the overall model in Eq. (9) for the piezo-actuated stage. The proposed identification processes focus mainly on the experimentally phenomenal data to obtain the overall model, which is different from identifying the parameter values in Eq. (9) one by one with specifically physical meaning. The mass-spring-damper model of the mechanical stage is also identified for better comparison with the overall model of the piezo-actuated stage. More details about the identification of the mechanical stage are presented in the Appendix.

The identification for the overall piezo-actuated stage including the power amplifier, the WPA, the mechanical stage and the capacitive sensor in Fig. 4 is executed in the frequency domain. The sinusoidal input voltage signal of a known frequency is generated from the AD5436A real-time platform

and then fed into the power amplifier to drive the piezo-actuated stage. The output displacement of the piezo-actuated stage is measured by the capacitive sensor and then captured in real time by the AD5436A real-time platform. The sampling period is 0.1 ms.

If the overall piezo-actuated stage is treated as a linear system, its displacement response to the sinusoidal voltage is also sinusoidal with the same frequency but different magnitude and phase. Suppose the sinusoidal input voltage and the corresponding output displacement of the overall stage can be expressed by $u = A_u \sin(2\pi ft) + \bar{u}$ and $x = A_x \sin(2\pi ft + \varphi) + \bar{x}$ respectively, where A_u, A_x and \bar{u}, \bar{x} are the magnitude and average (also referred as 'offset') values of the input and output sinusoid, and f is the frequency. Then the amplitude ratio $M = A_x/A_u$ and phase φ of the frequency response can be calculated in the following equation

$$\begin{aligned}
R_{uu}(0) &= \frac{1}{n} \sum_{i=1}^n (u(i)u(i)) \\
R_{xx}(0) &= \frac{1}{n} \sum_{i=1}^n (x(i)x(i)) \\
R_{ux}(0) &= \frac{1}{n} \sum_{i=1}^n (u(i)x(i)) \\
A_u &= \sqrt{2(R_{uu}(0) - \bar{u}^2)} \\
A_x &= \sqrt{2(R_{xx}(0) - \bar{x}^2)} \\
M &= \frac{A_x}{A_u} = \sqrt{\frac{R_{xx}(0) - \bar{x}^2}{R_{uu}(0) - \bar{u}^2}} \\
\varphi &= -\arccos\left(\frac{R_{ux}(0) - \bar{u}\bar{x}}{\sqrt{R_{uu}(0) - \bar{u}^2}\sqrt{R_{xx}(0) - \bar{x}^2}}\right)
\end{aligned} \tag{10}$$

where n is the number of the sampled steady-state output sinusoidal displacement.

In the practical calculation, n is usually a multiple of the data point number in one sinusoidal period. And the M and φ of the frequency response at a certain frequency can thus be computed via Eq. (10) using the logged data points $u(i), x(i), i = 1 \cdots n$. In general, M and φ are functions of the frequency of the input sinusoidal voltage. In the experimental implementation,

totally 76 frequencies are chosen as 0.5, 1, 2, 4, 6, \dots (arithmetic progression, increase by the same 2), 54, 55, 56, \dots , 60, 62, 64, \dots , 100, 125, 150, \dots , 500, 600, 700, \dots , 1000 Hz. Based on the measured data of frequency response, the transfer function of 6 order from the input voltage to the output displacement for the overall piezo-actuated stage can be identified using MATLAB System Identification Toolbox. Specially, the MATLAB function $G_{\text{if}} = \text{invfreqs}(h_{\text{if}}, w_{\text{if}}, n_{\text{if}}, m_{\text{if}}, wt_{\text{if}}, iter_{\text{if}}, tol_{\text{if}})$ is used [19], where $G_{\text{if}}(s)$ is the identified transfer function, $h_{\text{if}} = M \cos \varphi + jM \sin \varphi$ is the measured complex frequency response at the frequency point w_{if} , n_{if} and m_{if} are the identified numerator and denominator orders of the transfer function $G_{\text{if}}(s)$ respectively, wt_{if} is the weighting factor, $iter_{\text{if}}$ is the iteration number and tol_{if} is the bound value of the norm of the modified gradient vector for algorithm convergence. h_{if} , w_{if} and wt_{if} are usually vectors, and n_{if} , m_{if} , $iter_{\text{if}}$ and tol_{if} are generally scalars. This function adopts the damped Gauss-Newton method for iterative search in order to solve the direct problem of minimizing the weighted sum of the squared error between the actually measured and the identified frequency response points, i.e. $\min \sum_{i=1}^n (wt_{\text{if}}(i)|h_{\text{if}}(i) - G_{\text{if}}(e^{jw_{\text{if}}(i)})|^2)$. Based on the measured frequency response, the parameters of the identification function invfreqs are chosen as $n_{\text{if}} = 1$, $m_{\text{if}} = 6$, $wt_{\text{if}} = [1, 1, \dots]$, $iter_{\text{if}} = 50$ and $tol_{\text{if}} = 1 \times 10^{-8}$.

Some mathematical operations for preprocessing and post-processing are also used in order to obtain a better identified model [20]. The identified transfer function in the s domain is

$$\frac{x_s}{u_{in}} = \frac{1.144 \times 10^{17}s + 1.559 \times 10^{21}}{s^6 + 4460s^5 + 5.279 \times 10^7s^4 + 1.431 \times 10^{11}s^3 + 5.181 \times 10^{14}s^2 + 8.615 \times 10^{17}s} \quad (11)$$

The comparison between the measured data and the data from the identified model is shown in Fig. 5. The identified model can fit the measured data quite well.

5. Control and experimental results

During the process of closed-loop control design and experiments, the controlled plant is the overall piezo-actuated stage including the power amplifier, the WPA, the mechanical stage and the capacitive sensor. The control design is executed mainly in MATLAB/Simulink, and the control implementation is realized using the rapid control prototype (RCP) method based on the AD5436A real-time platform. The AD5436A real-time platform can run the

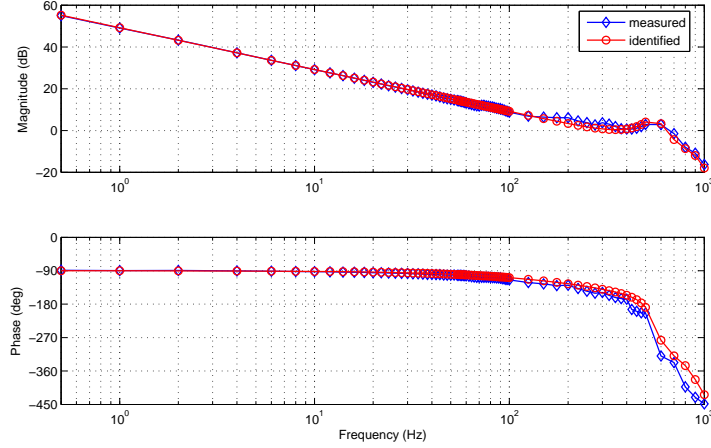


Figure 5: The comparison between the measured data and the data from the identified model.

generated C codes from the developed control algorithm model in Simulink. The closed-loop servo period T_s is 0.1 ms.

The root locus method is firstly used to decide the approximate maximum feedback loop gain. The root loci of the identified model in Eq. (11) with respect to the feedback loop gain is shown in Fig. 6. The maximum feedback loop gain should not exceed 0.625 for stability. The value can serve as a limitation of loop gain in the next positioning and tracking control.

5.1. PTP positioning control

PTP positioning can also be referred to as step displacement regulation. The desired displacement is usually a constant set point. The aim of PTP positioning control is to keep the displacement error small in a fast settling time. The hybrid control strategy including feedback and feed-forward control is adopted as shown in Fig. 7. The proportional-integral-derivative (PID) control serve as the feedback control taking the displacement error as the input. To avoid the sudden jump of the set point, the transient profile is constructed so that the overall stage can reasonably follow. From the Eq. (11), the overall piezo-actuated stage can be classified as the system of Type 1. Hence the feed-forward control is designed to be proportional to the velocity of the desired motion. The tracking differentiator is designed for the fastest tracking of the desired step motion.

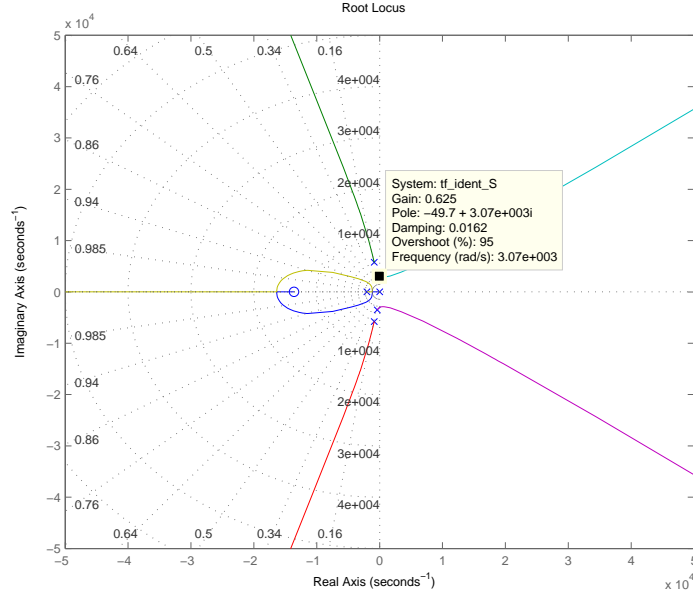


Figure 6: The root loci of the identified model in Eq. (11).

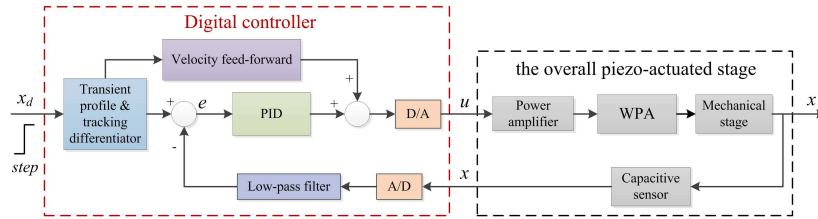


Figure 7: The control scheme for PTP positioning.

A discrete-time solution for the transient profile and tracking differentiator [21] can be obtained in the following equation:

$$\begin{aligned} x_1(k+1) &= x_1(k) + T_s v_1(k) \\ v_1(k+1) &= v_1(k) + T_s f_{han}(x_1(k) - x_d(k), v_1(k), a, T_s) \end{aligned} \quad (12)$$

where x_d is the desired step displacement and a is the controller parameter,

and the function $\text{fhan}(x_1, v_1, a, T_s)$ is defined as

$$\begin{aligned}
d &= T_s a^2, \quad a_0 = T_s v_1, \quad y = x_1 + a_0 \\
a_1 &= \sqrt{d(d + 8|y|)} \\
a_2 &= a_0 + \text{sign}(y)(a_1 - d)/2 \\
s_y &= (\text{sign}(y + d) - \text{sign}(y - d))/2 \\
\tilde{a} &= (a_0 + y - a_2)s_y + a_2 \\
s_a &= (\text{sign}(\tilde{a} + d) - \text{sign}(\tilde{a} - d))/2 \\
\text{fhan} &= -as_a \left(\frac{\tilde{a}}{d} - \text{sign}(\tilde{a}) \right) - a \text{sign}(\tilde{a}).
\end{aligned} \tag{13}$$

Eq. (12) and (13) provide a time-optimal solution which can guarantee the transient process from x_1 to x_d at the velocity of v_1 . And v_1 can be treated as the tracking differentiator whose derivative is subject to the acceleration limit a .

The simulink model for the real-time PTP positioning control experiment is illustrated in Fig. 8. The blocks *TPTD*, *kf*, *kp* and *ki* are used for the transient profile and tracking differentiator, feed-forward and feedback PID control, respectively. The block *IIR Filter* represents a low-pass infinite impulse response filter for reducing the noise of the capacitive sensor. The subsystem block *Subsys_DataStore* is utilized for experimental data recording. The subsystem block *AD5436A_Cfg* is used for the configuration of the AD5436A platform. Other blocks such as *Ext02A_DAOout* and *Ext01_ADIin* in the AD5436A target library provide real-time D/A and A/D interfaces to the AD5436A platform, through which the Simulink model can send the analog voltage signal to the power amplifier and collect the analog voltage signal from the capacitive sensor. In the experimental implementation, the Simulink model is automatically transformed into C codes by MATLAB Embedded Coder and then downloaded to the rapid control prototyping AD5436A platform for real-time execution. For the 300 μm step positioning, the parameters of the proposed controller as shown in Fig. 8 are $a = 4000000$, $k_f = 4.95 \times 10^{-5}$, $k_p = 0.046$ and $k_i = 0.005$, where a , k_f , k_p and k_i denote the transient profile acceleration limit, the feed-forward gain, the feedback proportional and integral gain. Besides, the low-pass filter is chosen to have the bandwidth of 100 Hz.

The experimental result is shown in Fig. 9. For the PTP positioning control application, the settling time t_s is defined in this paper to be the

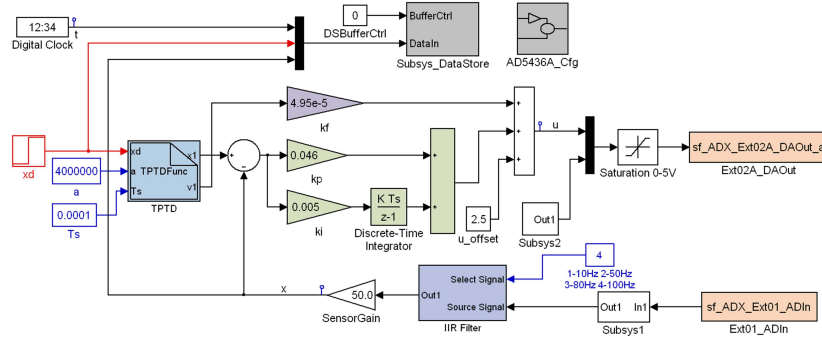


Figure 8: The Simulink model for PTP positioning control.

time needed to settle within the displacement sensor resolution (25 nm). t_s for the 300 μm step positioning of the proposed controller is 0.12 s and the overshoot is 1.3 μm . The settling time for the other different steps of 1, 10 and 100 μm are 0.04, 0.085 and 0.1 s respectively, whose figures are not illustrated for the succinctness of this paper. It is worth noting that, compared with the results in Refs. [12] and [13], t_s for the 100 μm step are 0.6 and 0.4 s respectively, which are longer than that of this paper. Hence the comparisons imply the excellent performance of faster settling time of the proposed controller.

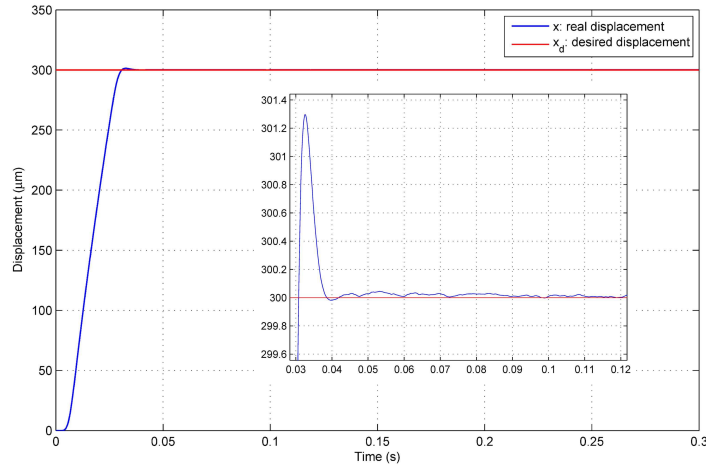


Figure 9: The experimental result of PTP positioning control for 300 μm step.

5.2. Sinusoidal trajectory tracking control

The aim of trajectory tracking control is to cause the output displacement to follow the reference input as closely as possible. Sinusoidal trajectory is chosen because other more complex trajectories can be described by the sinusoidal components over an interesting band of frequencies. The hybrid control strategy including feedback, feed-forward and repetitive control is developed as shown in Fig. 10. Different from Fig. 7, the direct differentiator is used to obtain the velocity of the sinusoidal reference input x_d with continuous trajectory. Besides, a discrete-time RC is designed to be plugged into the feedback controller to enhance the periodic trajectory tracking performance. RC can be easily implemented in practice and its initial states need not be the same at the start of each iteration [4, 16, 17].

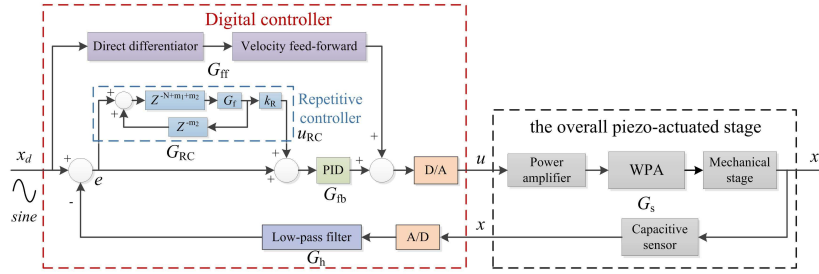


Figure 10: The control scheme for sinusoidal trajectory tracking.

As illustrated in Fig. 10, RC generally comprises a pure delay z^{-N} , two phase-lead compensator units z^{m_1} and z^{m_2} , a filter G_f with a unit gain, and a gain k_R . N denotes the number of sampled data points during one period of the desired trajectory x_d . It can be calculated as $N = T_d/T_s$, where T_d is the period duration time. z^{m_1} is added to improve the tracking performance of the RC. z^{m_2} is added to increase the stability margin of the RC. G_f is in fact necessary for stabilizing the RC. k_R is designed for trade-off tuning of convergence and performance of the RC. G_{ff} , G_{fb} and G_h represent the transfer functions of the feed-forward controller, the feedback PID controller and the low-pass filter for the capacitive sensor in the z -domain respectively, while G_s represents the transfer function of the overall piezo-actuated stage. The transfer function $G_{RC}(z)$ of the RC from e to u_{RC} can be derived as

$$G_{RC}(z) = \frac{u_{RC}(z)}{e(z)} = \frac{k_R G_f(z) z^{-N+m_1+m_2}}{1 - G_f(z) z^{-N+m_1}}. \quad (14)$$

If necessary, the variable z of transfer functions in the z -domain will be omitted for the sake of brevity in the following paragraphs. G_f is designed with the discrete-time transfer function in the following equation

$$G_f = \frac{(1 - \alpha)z}{z - \alpha}, 0 < \alpha < 1. \quad (15)$$

The transfer function G_{oc} of the proposed overall controller in Fig. 10 from x_d to x is

$$G_{oc} = \frac{x(z)}{x_d(z)} = \frac{G_s (G_{fb} (1 + G_{RC}) + G_{ff})}{1 + G_s G_h G_{fb} (1 + G_{RC})}. \quad (16)$$

By substituting the zero for G_{RC} , the transfer function \bar{G}_{oc} of the proposed overall controller without the RC can be obtained as

$$\bar{G}_{oc} = \frac{G_s (G_{fb} + G_{ff})}{1 + G_s G_h G_{fb}}. \quad (17)$$

The sensitivity functions $\bar{S} = \bar{S}_{G_s}^{\bar{G}_{oc}}$ and $S = S_{G_s}^{G_{oc}}$ of \bar{G}_{oc} and G_{oc} to G_s can thus be derived respectively as

$$\begin{aligned} \bar{S} &= \frac{1}{1 + G_s G_h G_{fb}} \\ S &= \frac{1}{1 + G_s G_h G_{fb} (1 + G_{RC})} \\ &= \frac{1}{1 + G_s G_h G_{fb}} \cdot \frac{1}{1 + \frac{G_s G_h G_{fb}}{1 + G_s G_h G_{fb}} G_{RC}} \\ &= \bar{S} \cdot \frac{1}{1 + (1 - \bar{S}) G_{RC}}. \end{aligned} \quad (18)$$

Using Eq. (14) to replace G_{RC} in Eq. (18), S becomes

$$S = \bar{S} \cdot \frac{1 - G_f z^{-N+m_1}}{1 - G_f z^{-N+m_1} (1 - (1 - \bar{S}) k_R z^{m_2})}. \quad (19)$$

Therefore, based on the small-gain theorem [17], the asymptotic stability condition of the designed sinusoidal trajectory tracking controller with the RC can be given as:

1. All the poles of the sensitivity function $\bar{S}(z)$ lie inside the open unit circle of the complex plane.
2. $|G_f(z) (1 - (1 - \bar{S}(z)) k_R z^{m_2})|_{z=e^{j\omega T_s}} < 1$ with $\omega \in [0, \pi/T_s]$.

The simulink model for the sinusoidal trajectory tracking control experiment is shown in Fig. 11. The blocks *Delay_nm1m2*, *Gf*, *Delay_m2* and *kR* together serve as the function of the RC. The block *Discrete Derivative* represents a direct differentiator in discrete time. The other identical blocks with those in Fig. 8 are designed having the same functions. For the desired sinusoidal trajectory $x_d = 50 \sin(5\pi t - \pi/2) + 50 \mu\text{m}$, the parameters of the proposed controller as illustrated in Fig. 11 are chosen as $N = 4000$, $m_1 = 50$, $m_2 = 0$, $\alpha = 0.995$, $k_R = 0.8$, $k_f = 3.575 \times 10^{-4}$, $k_p = 0.11$ and $k_i = 0.005$.

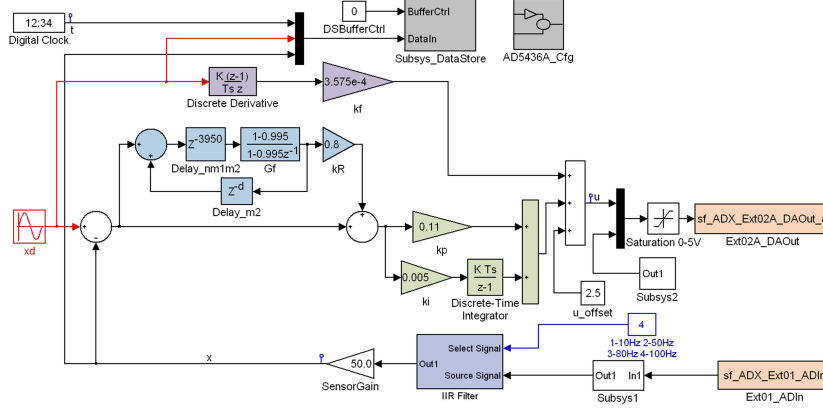


Figure 11: The Simulink model for the sinusoidal trajectory tracking control.

The experimental result is shown in Fig. 12. For the sinusoidal trajectory tracking control application, the following displacement tracking errors are defined as the criteria for the control performance: $e_i = x_d(i) - x(i)$, $e_{ma} = \max(|e_i|)$, $e_{rms} = \sqrt{(\sum_{i=1}^n e_i^2)/n}$, $e_{MA} = (\sum_{i=1}^n e_i)/n$, $e_{MSD} = \sqrt{(\sum_{i=1}^n (e_i - e_{MA})^2)/n}$ and $e_{mr} = e_{ma}/\max(|x_d|)$. For the $x_d = 50 \sin(5\pi t - \pi/2) + 50 \mu\text{m}$ tracking of the developed hybrid controller with RC, the errors e_{ma} , e_{rms} , e_{MA} , e_{MSD} and e_{mr} are 1.9938, 1.2053, -0.0255, 1.2051 μm and 1.99% respectively.

6. Conclusions

In this paper, a dynamic model is firstly investigated for a flexible mechanical stage driven by the WPA. Then the proposed model is identified

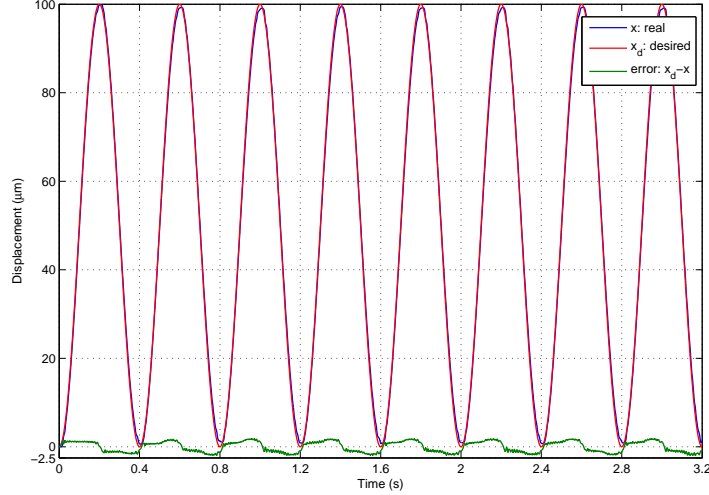


Figure 12: The experimental result of the sinusoidal trajectory tracking control.

based on the open-loop frequency response data. Finally, hybrid closed-loop controllers are designed. The transient profile and tracking differentiator is proposed for quick settling of PTP positioning control, and the discrete-time RC is adopted to enhance the tracking precision for the periodic sinusoidal trajectory. For the $300 \mu\text{m}$ PTP positioning, the settling time is 0.12 s to keep the steady error within 25 nm . And for the sinusoidal trajectory of $50 \mu\text{m}$ amplitude, the maximum tracking error is 1.99% . Future work will take into consideration the non-linear hysteresis and friction characteristics of the piezo-actuated stage and design the corresponding control strategies.

Acknowledgements

This research is supported by the National Natural Science Foundation of China (No. 61504142 and 61604150).

Appendix

The identification for the mechanical stage is executed based on the experimental platform in Fig. 4. Because only the mechanical stage is in interest, the WPA is not connected with the mechanical stage. That is to say, the mechanical stage is isolated from the WPA, and the input for identification

is not the electrical voltage signal. In the experiment implementation, the PCB SN32048 hammer from PCB Piezotronics Company is used for the impulse force generation. The impulse force is then input to the mechanical stage, and the displacement response values are measured by the capacitive sensor. The applying direction of the impulse force is the same as the motion direction of the stage. Herein, the AD5436A real-time platform runs for the high-speed measurement purpose in 0.1 ms sampling period and captures the sensor displacement in real time. Based on the logged data of the displacement response to the impulse force, the first-order natural frequency and damping characteristics of the mechanical stage can be approximately computed in the following equation [22]

$$\xi_s = \frac{\ln \frac{x_n}{x_{n+1}}}{\sqrt{4\pi^2 + \left(\ln \frac{x_n}{x_{n+1}}\right)^2}} = \frac{c_s}{2\sqrt{m_s k_s}}$$

$$f_s = \frac{1}{T_{im} \sqrt{1 - 2\xi_s^2}} = \frac{1}{2\pi} \sqrt{\frac{k_s}{m_s}}$$

where ξ_s and f_s are the damping ratio and first-order natural frequency of the mechanical stage, x_n and x_{n+1} are the n th adjoining amplitudes of the displacement response waveform, and T_{im} is the period time of the displacement response waveform.

From the displacement data in Fig. .13 captured in the impulse response experiment, $\xi_s = 9.16 \times 10^{-4}$ and $f_s = 56.34$ Hz can be computed. $\xi_s = 9.16 \times 10^{-4}$ indicates that the damping value of the mechanical stage alone is very small. The flexure hinges introduce mainly elastic stiffness to the mechanical stage. There are not other elements with big or medium damping values in the mechanical stage. $f_s = 56.34$ Hz shows that the natural frequency of the mechanical stage is a little low, mainly because the displacement range of the mechanical stage can reach up to 500 μm .

References

- [1] P. Li, P. Li, Y. Sui, Adaptive fuzzy hysteresis internal model tracking control of piezoelectric actuators with nanoscale application, IEEE Transactions on Fuzzy Systems 24 (5) (2016) 1246 – 1254.

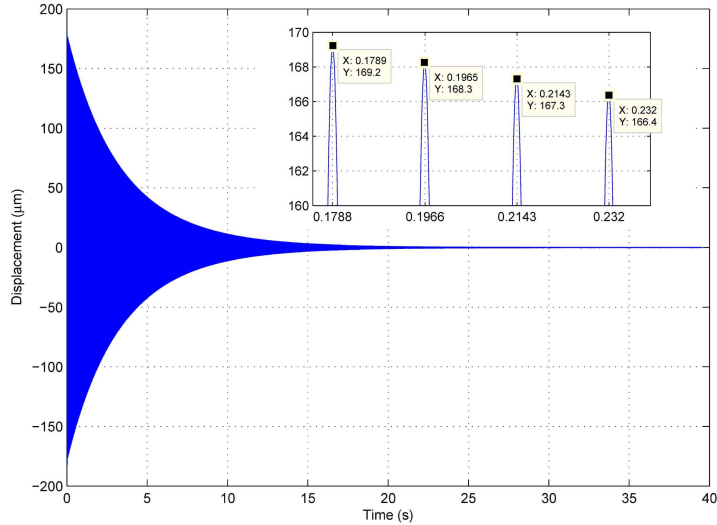


Figure .13: Displacement response of the mechanical stage to the impulse force.

- [2] P. Li, F. Yan, C. Ge, X. Wang, L. Xu, J. Guo, P. Li, A simple fuzzy system for modelling of both rate-independent and rate-dependent hysteresis in piezoelectric actuators, *Mechanical Systems and Signal Processing* 36 (1) (2013) 182 – 192.
- [3] C.-X. Li, G.-Y. Gu, L.-M. Zhu, C.-Y. Su, Odd-harmonic repetitive control for high-speed raster scanning of piezo-actuated nanopositioning stages with hysteresis nonlinearity, *Sensors and Actuators A: Physical* 244 (2016) 95 – 105.
- [4] P.-Z. Li, F. Yan, Repetitive control of piezoelectric actuators with fuzzy hysteresis compensation in nanopositioning applications, in: *16th International Conference on Mechatronics Technology*, Elsevier, Tianjin, China, 2012, pp. 533 – 537.
- [5] T.-W. Na, J.-H. Choi, J.-Y. Jung, H.-G. Kim, J.-H. Han, K.-C. Park, I.-K. Oh, Compact piezoelectric tripod manipulator based on a reverse bridge-type amplification mechanism, *Smart Materials and Structures* 25 (9) (2016) 095028.
- [6] C. Lin, Z. Shen, Z. Wu, J. Yu, Kinematic characteristic analysis of a

- micro-/nano positioning stage based on bridge-type amplifier, *Sensors and Actuators A: Physical* 271 (2018) 230 – 242.
- [7] P.-Z. Li, X.-D. Wang, Y.-X. Sui, D.-F. Zhang, D.-F. Wang, L.-J. Dong, M.-Y. Ni, Piezoelectric actuated phase shifter based on external laser interferometer: design, control and experimental validation, *Sensors* 17 (4) (2017) 838.
- [8] A. S. Bezryadina, D. C. Preece, J. C. Chen, Z. Chen, Optical disassembly of cellular clusters by tunable tug-of-war tweezers, *Light: Science & Applications* 5 (2016) e16158.
- [9] X. Chen, C. Chardin, K. Makles, C. Car, S. Chua, R. Braive, I. Robert-Philip, T. Briant, P.-F. Cohadon, A. Heidmann, T. Jacqmin, S. Delglise, High-finesse FabryPerot cavities with bidimensional Si₃N₄ photonic-crystal slabs, *Light: Science & Applications* 6 (2016) e16190.
- [10] Z.-Y. Zhou, Y. Li, D.-S. Ding, W. Zhang, S. Shi, B.-S. Shi, G.-C. Guo, Orbital angular momentum photonic quantum interface, *Light: Science & Applications* 5 (2016) e16019.
- [11] F. Szufnarowski, A. Schneider, Two-dimensional dynamics of a quasi-static legged piezoelectric actuator, *Smart Materials and Structures* 21 (2012) 055007 – 19.
- [12] R. J. E. Merry, N. C. T. de Kleijn, M. J. G. van de Molengraft, M. Steinbuch, Using a walking piezo actuator to drive and control a high-precision stage, *IEEE/ASME Transactions on Mechatronics* 14 (1) (2009) 21 – 31.
- [13] T. Uzunovic, E. Golubovic, A. Sabanovic, Piezo LEGS driving principle based on coordinate transformation, *IEEE/ASME Transactions on Mechatronics* 20 (3) (2015) 1395 – 1405.
- [14] R. Merry, D. Kessels, W. Heemels, M. van de Molengraft, M. Steinbuch, Delay-varying repetitive control with application to a walking piezo actuator, *Automatica* 47 (2011) 1737 – 1743.
- [15] F. Szufnarowski, A. Schneider, Force control of a piezoelectric actuator based on a statistical system model and dynamic compensation, *Mechanism and Machine Theory* 46 (2011) 1507 – 1521.

- [16] U. Aridogan, Y. Shan, K. K. Leang, Design and analysis of discrete-time repetitive control for scanning probe microscopes, *Journal of Dynamic Systems, Measurement, and Control* 131 (2009) 061103–1 – 061103–12.
- [17] M. Steinbuch, S. Weiland, T. Singh, Design of noise and period-time robust high-order repetitive control, with application to optical storage, *Automatica* 43 (2007) 2086 – 2095.
- [18] PiezoMotor, www.piezomotor.com.
- [19] MATLAB, www.mathworks.com.
- [20] L. Ljung, *System Identification: Theory for the User*, 2nd Edition, PTR Prentice Hall, Upper Saddle River, NJ, 1999.
- [21] J. Han, From PID to active disturbance rejection control, *IEEE Transactions on Industrial Electronics* 56 (3) (2009) 900 – 906.
- [22] R. W. Clough, J. Penzien, *Dynamics of Structures*, 2nd Edition, Computers and Structures Inc., 2010.